Journal of Geophysical Research: Atmospheres

RESEARCH ARTICLE
10.1029/2018JD029427

Dynamical Drivers of the Local Wind Regime in a Himalayan Valley

Emily R. Potter[1,2], **Andrew Orr**[1], **Ian C. Willis**[2], **Daniel Bannister**[1,3], **and Franco Salerno**[4]

[1]British Antarctic Survey, Cambridge, UK, [2]Scott Polar Research Institute, University of Cambridge, Cambridge, UK, [3]Satavia Ltd., Cambridge, UK, [4]Water Research Institute (IRSA-CNR), National Research Council, Brugherio, MB, Italy

Key Points:
- The atmospheric model represents the diurnal cycle of local valley winds well, with strong daytime up-valley winds and weak nighttime winds
- The dominant physical drivers of the valley circulation come from the pressure gradient, advection, and turbulent vertical mixing
- There is a consistent diurnal cycle in the drivers of the wind acceleration, but they are spatially variable and also affected by glaciers

Correspondence to:
E. R. Potter,
empott15@bas.ac.uk

Citation:
Potter, E. R., Orr, A., Willis, I. C., Bannister D., & Salerno, F. (2018). Dynamical drivers of the local wind regime in a Himalayan valley. *Journal of Geophysical Research: Atmospheres*, *123*, 13,186–13,202. https://doi.org/10.1029/2018JD029427

Received 1 AUG 2018
Accepted 8 NOV 2018
Accepted article online 12 NOV 2018
Published online 6 DEC 2018

Abstract Understanding the local valley wind regimes in the Hindu-Kush Karakoram Himalaya is vital for future predictions of the glacio-hydro-meteorological system. Here the Weather Research and Forecasting model is employed at a resolution of 1 km to investigate the forces driving the local valley wind regime in a river basin in the Nepalese Himalaya, during July 2013 and January 2014. Comparing with observations shows that the model represents the diurnal cycle of the winds well, with strong daytime up-valley winds and weak nighttime winds in both months. A momentum budget analysis of the model output shows that in the summer run the physical drivers of the near-surface valley wind also have a clear diurnal cycle, and are dominated by the pressure gradient, advection, and turbulent vertical mixing, as well as a nonphysical numerical diffusion term. By contrast, the drivers in the winter run have a less consistent diurnal cycle. In both months, the pressure gradient, advection, numerical diffusion, and Coriolis terms dominate up to 5,000 m above the ground. The drivers are extremely variable over the valley, and also influenced by the presence of glaciers. When glaciers are removed from the model in the summer run, the wind continues further up the valley, indicating how the local valley winds might respond to future glacier shrinkage. The spatial variability of the drivers over both months is consistent with the complex topography in the basin, which must therefore be well represented in weather and regional climate models to generate accurate outputs.

Plain Language Summary The rain and snow in Himalayan valleys, and the formation and melting of glaciers, are affected by the wind in the valleys. Exactly what drives this wind is not fully understood. Around the world, wind in valleys generally travels up the valley, and up the sides of mountains, during the day. This is due to the sun heating different areas by different amounts, creating areas of low and high air pressure. Here we use a computer simulation to determine whether the difference in pressure is the main cause of the acceleration of the wind in a valley in the Himalayas, or whether there are other forces which also affect the wind. We compare the simulation to measurements taken in the valley. We find that the pressure difference is the main process affecting the acceleration of the wind. However, the winds in the valley are also driven by the effects of turbulence and affected by the shape of the valley. The forces are consistent over the month, accelerating the wind in the morning and decelerating the wind in the afternoon every day.

1. Introduction

Approximately 800 million people depend on water resources originating from the Hindu-Kush Karakoram Himalayan (HKKH) region (Pritchard, 2017), attributable to both rainfall and melting of snow and ice. Understanding the local valley wind regime in this region is key to better understanding the drivers of its glacio-hydro-meteorological system. The summer monsoon is the predominant large-scale driver of precipitation in the eastern areas of the HKKH (Shea, Wagnon, et al., 2015; Wagnon et al., 2013; Yang et al., 2017), while in the western areas it is the winter westerly disturbances (Ueno et al., 2008). In addition to the synoptic scale systems, the local valley wind regimes also affect precipitation by transporting moisture and clouds up the slopes and valleys during the day, especially at high altitudes (Bollasina et al., 2002; Egger et al., 2002; Karki et al., 2017; Orr et al., 2017; Shea, Wagnon, et al., 2015; Tartari et al., 1998). They also affect snow redistribution (Wagnon et al., 2013). The local valley winds and associated clouds additionally affect the radiation reaching the snow and ice (Shea, Wagnon, et al., 2015) and near-surface temperature (Immerzeel et al., 2014). Thus,

the local wind regime plays an important role, ultimately, in glacier accumulation, ablation, and therefore mass balance.

Two important thermal wind mechanisms that occur in valleys worldwide are those that cause slope winds and valley winds (Whiteman, 2000; Zardi & Whiteman, 2013). Slope winds blow upslope during the day and downslope at night. They are caused by the heating (cooling) of the ground during the day (night), leading to a local horizontal pressure difference between the air at the slope surface and at the same altitude away from the slope. Valley winds blow along the valley axis, up-valley during the day and down-valley at night. They are formed by the unequal heating of the air in the valley or between the valley and the wider surroundings, also leading to a pressure difference. We will refer collectively to the winds on the slopes and in the valleys, including these two mechanisms, as the local valley wind regime.

The scarcity of weather stations and detailed modeling studies in the HKKH region means that there are still considerable uncertainties surrounding our understanding of its local valley wind regime. The presence of a local wind regime has been previously documented in valleys in this region (Inoue, 1976; Ohata et al., 1981; Shea, Wagnon, et al., 2015; Ueno et al., 2001, 2008; Yang et al., 2017; Zängl et al., 2001). However, few studies have investigated the forces driving the local wind regime. Sun et al. (2018) found that horizontal pressure gradients are crucial in the formation of the wind in the Arun Valley, Nepal. Zängl et al. (2001) found that topography and moisture affect pressure gradients driving the local winds in the Kali Gandaki Valley, Nepal, suggesting that there are complex interactions between the forces accelerating the wind. Therefore, further research is needed into the magnitude of the pressure gradient force, as well as the influence of other physical forces driving the wind acceleration, such as advection, the rotation (Coriolis effect) and curvature of the Earth, and turbulent vertical mixing. In addition, Yang et al. (2017) point to the need for high-resolution modeling studies investigating the effects of the glaciers on the local valley wind.

To investigate the dynamical drivers of the local valley winds in the HKKH region, this study will undertake a detailed momentum budget analysis of output from the Weather Research and Forecasting (WRF) model applied to the Dudh Koshi river basin in the Nepalese Himalaya, during July 2013 and January 2014. In addition to the seasonal differences, we investigate the extent to which glaciers impact the local acceleration of the wind regime. On a large scale, momentum budget analysis of output from models has been used to analyze slope winds over the Antarctic and Greenland ice sheets (Renfrew, 2004; van Angelen et al., 2011; van den Broeke et al., 2002). On a smaller scale, it has been used with the WRF model at high horizontal resolution to determine the role of the pressure gradient in forming a cross-valley circulation in a crater (Lehner & Whiteman, 2014).

An improved understanding of the wind dynamics in valleys in the HKKH region will increase understanding of the fundamental meteorological interactions in the local climate system. The subsequent improved representation of air flow in atmospheric models will result in better predictions of important meteorological variables such as temperature, humidity, radiation, and precipitation, which are required as inputs to hydrology and glacier models (Widmann et al., 2017).

2. Observations, Model, and Method

2.1. Location and Observational Data

The Dudh Koshi river basin is in the eastern Nepalese Himalaya along the southern slopes of Mt Everest (Figure 1a) and includes the Khumbu region. The altitude ranges from a few hundred meters above sea level (m asl) to the top of Mt Everest at 8,848 m asl (Figure 1b). In the lower regions the valley is forested, turning to bare rock with glaciers across the higher altitude areas (Magnani et al., 2018). Approximately 25% of the glacierized area is debris-covered (Salerno et al., 2017; Shea, Immerzeel, et al., 2015). There is a strong seasonal and diurnal cycle of temperature, wind, and precipitation (Shea, Wagnon, et al., 2015). The local wind regime is characterized by up-valley winds during the day throughout the year, with weak up-valley winds at night during the monsoon season and some evidence of down-valley winds at night in the winter (Inoue, 1976; Ohata et al., 1981; Shea, Wagnon, et al., 2015; Ueno et al., 2001; Yang et al., 2017).

There are two automatic weather stations (AWSs) used in this study, at Namche (3,570 m asl) and Pheriche (4,260 m asl) (see Figure 1b for locations). Both AWSs are located on the valley floor. See Yang et al. (2017) for a full description of their locations and instrumentation. The sensors for the wind measurements were supplied by LSI-Lastem (Italy). In addition, full details of the AWS measurements are given at http://geonetwork.evk2cnr.org. Hourly measurements of wind speed and direction are used for this analysis.

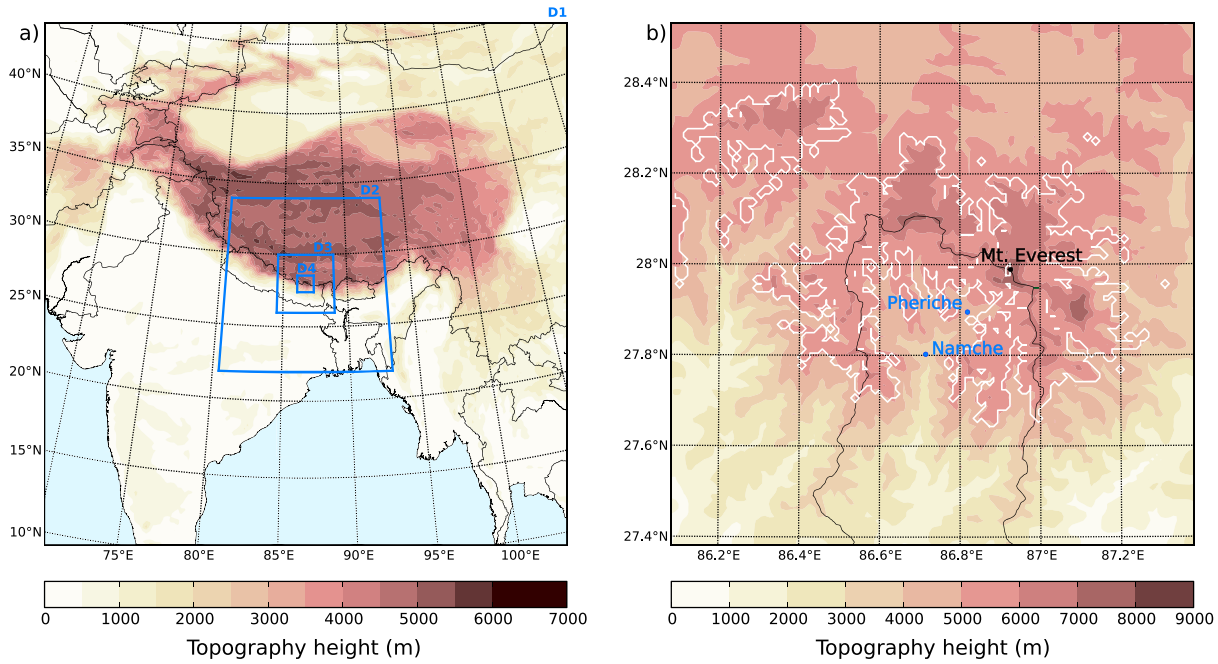

Figure 1. (a) The geographical extent of the four model domains (labeled D1 to D4) and the topographic height of the outer domain (m; shading). (b) The innermost 1 km domain (D4) showing the topographic height (m; shading), the watershed outline of the Dudh Koshi river basin (solid black line), the extent of the permanent snow and ice in the model (solid white line), and the location of the automatic weather stations at Namche and Pheriche (solid blue circles). The location of Mount Everest is also shown for reference (solid black circle).

Note that over 50% of the data are missing for Namche in January, and a single hour is missing at Pheriche in July. A visual inspection of the data showed a characteristic diurnal cycle over the month, with no outliers.

Yang et al. (2017) analyzed the diurnal cycle in the wind at Namche and Pheriche between 2007 and 2011, and found that the average minimum (maximum) meridional wind velocity in the monsoon season was approximately 0.5 (3.5) and 1 (6) m/s at Namche and Pheriche, respectively. This study finds that the approximate average minimum (maximum) wind speeds for July 2013 are 0.7 (4.4) m/s at Namche and 1 (4.6) m/s at Pheriche, and so July 2013 is broadly representative of the monsoon season in recent years. Equivalent values for the winter months were not available from Yang et al. (2017).

2.2. Atmospheric Model

Two month-long runs were conducted using version 3.8.1 of the WRF model (Skamarock et al., 2008) over the Dudh Koshi river basin for July 2013 and January 2014 (hereafter referred to as the *summer* and *winter* runs, respectively). Previous high-resolution modeling studies in the Nepalese Himalaya suggest that a horizontal resolution of around 1 km is necessary to accurately represent valley winds (Collier & Immerzeel, 2015; Karki et al., 2017; Orr et al., 2017). This is selected, therefore, as the resolution of the innermost domain, which is nested within three other domains at resolutions of 27, 9, and 3 km (Figure 1a). The model has 50 vertical levels from the surface to 50 hPa, with around seven levels located in the lowest kilometer. The default U.S. Geological Survey WRF topography in the innermost domain has been replaced with 90 m resolution topography from the Shuttle Radar Topography Mission (Jarvis et al., 2008). The permanent snow and ice is poorly represented in the default U.S. Geological Survey WRF land use over HKKH (Collier & Immerzeel, 2015; Orr et al., 2017), and so is adjusted in the innermost two domains to match the Randolph Glacier Inventory (Consortium, 2015). Debris cover is not currently represented in the WRF model. Most of the physics and dynamics options have been chosen following those used in Collier and Immerzeel (2015), however the microphysics scheme has been chosen following the results and recommendations of Orr et al. (2017). The model is initialized and forced by ERA-Interim data at the boundary (Dee et al., 2011) and the spin-up period is 14 days. For full model details, see Table 1.

To compare the model to the AWS wind measurements, the hourly 10 m model wind speeds at the nearest grid points to the two AWS locations are selected. The observational data are adjusted to a height of 10 m by assuming conditions of neutral stability and using a logarithmic profile, as suggested in Whiteman (2000).

Table 1
Details of the Weather Research and Forecasting Model Set-Up

Domains and forcing data	
Number of domains	4
Horizontal grid resolution (km)	27, 9, 3, 1
Number of vertical levels	50
Model top	50 hPa
Topography data	Domains 1, 2, & 3: U.S. Geological Survey 30 s; domain 4: Shuttle Radar Topography Mission (Jarvis et al., 2008)
Land surface and snow and ice data	Domains 1 & 2: U.S. Geological Survey 30 s; domains 3 & 4: U.S. Geological Survey 30 s, adjusted using the Randolph Glacier Inventory (Consortium, 2015)
Forcing data	ERA-Interim (Dee et al., 2011)
Spin-up period	14 days
Physics schemes	
Microphysics	Morrison double-moment (Morrison et al., 2009)
Radiation	CAM scheme (Collins et al., 2004)
Surface layer	Revised MM5 (Jiménez et al., 2012)
Land surface	Noah-MP (multi-physics) (Niu et al., 2011)
Planetary boundary layer	Mellor-Yamada Nakanishi and Niino level 2.5 (Nakanishi & Niino, 2004)
Cumulus	Domains 1 & 2: Kain-Fritsch (Ma & Tan, 2009); domains 3 & 4: none
Dynamics	
Diffusion	Calculated in real space
Eddy diffusion coefficient	Diagnosed from horizontal diffusion
Short-wave numerical noise filter	On
Top of model damping	Rayleigh damping in top 5,000 m of model
Time off-centering for vertical sound waves	Set to 1

This calculation requires an estimate of the surface roughness length (z_0) of the terrain, which is assumed to be 0.25 m high grass in the summer with $z_0 = 0.04$ m (Oke, 2002), and snow covered during winter with $z_0 = 0.001$ m (Oke, 2002). All results are in local time (LT; UTC+5:45 hr), and only the results of the Dudh Koshi river basin, in the innermost 1 km domain, are analyzed.

To investigate the effects of glacier cover on the local valley wind, the model runs are repeated but with all permanent snow and ice (referred to as the glacierized region) removed by changing the land classification to barren ground and the underlying soil type from land ice to rock. No other aspects of the model are changed, and snow can still fall during the run. The experiments with the glacierized region removed will be referred to as the *perturbation experiments*.

To test for statistical significance in the change in the wind velocity when the glacierized region is removed from the model, a two-tailed Student's *t* test was conducted at each point in the domain. To account for the effects of autocorrelation, we calculate the effective sample size at each point in the domain using the method described in Chandler and Scott (2011). The effective *t* statistic is calculated using the method described in von Storch and Zwiers (1999). The meridional and zonal velocities are tested separately for significance and the wind vector is deemed significant if there is significance in either direction. To account for the increased chance of incorrectly rejecting the null hypothesis when being tested in the meridional or zonal direction, in each direction the significance level is set to $1 - \sqrt{0.95} = 0.0253$, to give an overall significance at the 5% level. This arises from solving $2(1 - n)n + n^2 = 0.05$, where n is the probability of incorrectly rejecting one or the other of the null hypotheses. The output from the summer run and the experiment without permanent snow and ice are treated as independent. A bootstrap method (von Storch & Zwiers, 1999) was also employed

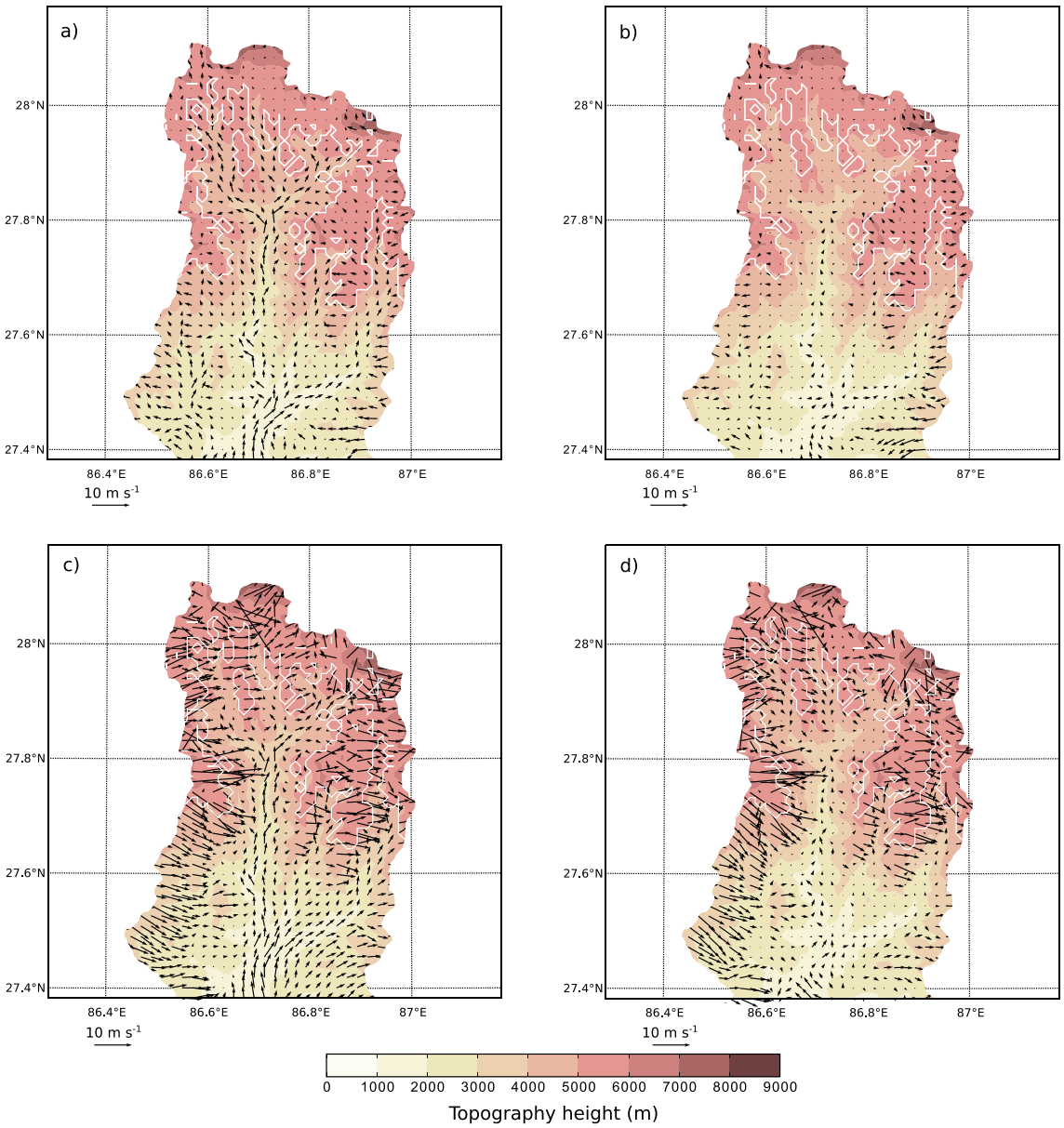

Figure 2. The monthly averaged daytime (06:00–18:00 LT) (a) and nighttime (19:00–05:00 LT) (b) 10 m model winds (m/s; vectors) for July 2013 for the Dudh Koshi river basin. Panels (c)–(d) are as (a)–(b), but for January 2014 (daytime is taken as 07:00–17:00 LT in the winter run, nighttime as 18:00–06:00 LT). Wind vectors are displayed at every second model grid point (every 2 km) for clarity. Also shown are the model topographic height (m; shading) and the extent of the permanent snow and ice in the model (solid white line).

to confirm the significance. This produced a very similar result to the *t* test, and only the data points which were significant in both tests are shown as significant in section 3.3.

2.3. Momentum Budget

The dynamics in the WRF model are based on the moist flux-form nonhydrostatic Euler equations (Skamarock et al., 2008). The horizontal momentum components of these equations are

$$\partial_t U = -\nabla \cdot \mathbf{V}u - (\mu_d \alpha \partial_x p + (\alpha/\alpha_d)\partial_\eta p \partial_x \phi) + F_U, \tag{1}$$

$$\partial_t V = -\nabla \cdot \mathbf{V}v - (\mu_d \alpha \partial_y p + (\alpha/\alpha_d)\partial_\eta p \partial_y \phi) + F_V. \tag{2}$$

Here $\mu_d(x, y)$ is the mass of dry air in the column and p is the pressure. The coupled wind velocity $\mathbf{V} = (U, V, W) = \mu_d \mathbf{v}$, where U and V are the mass coupled zonal and meridional velocities and W is the mass

coupled vertical velocity, and $\mathbf{v} = (u, v, w)$ is the uncoupled velocity. The vertical coordinate used by WRF is given by $\eta = (p_{dh} - p_{dht})/\mu_d$, where p_{dh} is the hydrostatic pressure of the dry atmosphere and p_{dht} represents this value at the top of the model. ϕ is the geopotential. $\nabla\cdot$ is the divergence. The inverse density of dry air is given by α_d, with $\alpha = \alpha_d(1 + q_v + q_c \ldots)^{-1}$ where q_v, q_c are the mixing ratios of vapor and cloud, respectively. The ∂_* sign denotes partial differentiation with respect to subscript *. See Skamarock et al. (2008) for further details.

In equation (1) the zonal wind component of the mass coupled acceleration at a fixed point in space is represented by $\partial_t U$. The advection term is given by $-\nabla \cdot \mathbf{V}u$. The forcing term F_U represents acceleration due to the effects of Coriolis and curvature, horizontal and numerical diffusion, and the contribution from model physics, which here arises from subgrid scale turbulent vertical mixing, hereafter referred to as turbulent vertical mixing. The term $-(\mu_d \alpha \partial_x p + (\alpha/\alpha_d)\partial_\eta p \partial_x \phi)$ represents the pressure gradient force. The effects of damping at the top of the model have been ignored as these only affect the winds in the stratosphere (not shown). Equation (2) is analogous to equation (1), but for the meridional wind component. The advection, Coriolis, curvature, horizontal diffusion, numerical diffusion, turbulent vertical mixing, and pressure gradient terms were extracted from the WRF model using code adapted from Moisseeva (2014) and following the method suggested by Lehner (2012).

The pressure gradient is predominantly caused by gradients in potential temperature, and its effects close to the ground are highly dependent on topography (Moisseeva & Steyn, 2014; Skamarock et al., 2008). It is driven by both synoptic scale temperature differences and the local temperature differences which contribute to slope and valley winds. Advection is related to the horizontal and vertical differences in wind velocity, and represents, therefore, the influence of the surrounding wind on the wind at the point being measured. Turbulent vertical mixing acts throughout the atmospheric column (Skamarock et al., 2008). Numerical diffusion is a nonphysical parameter which is added for model stability, necessary over the complex topography. In the following analysis, all forces have been divided by the mass of dry air in the column and are therefore represented as the components of acceleration (i.e., $\partial_t u$, $\partial_t v$).

3. Results

3.1. Summer

Figures 2a and 2b demonstrate a clear diurnal cycle in the model 10 m winds over the Dudh Koshi river basin during the summer, with strong up-valley winds during the daytime (averaged between 06:00 and 18:00 LT), and much weaker but still upslope winds during the nighttime (averaged between 19:00 and 05:00 LT). The upslope winds are damped over the high-elevation glacierized regions of the valley. At Namche (Figures 3a–3c) and Pheriche (Figures 3d–3f), the model generally represents the observed wind speed and direction well, as evidenced by the low root-mean-square error values of 1.32 and 1.5 m/s, respectively. However, the daytime peak wind speed occurs later in the model than in the observations at Namche and is slightly underestimated, and is underestimated at Pheriche (Figures 3c and 3f, respectively). Wind speeds are approximately 4 m/s during the day, and approximately 1 m/s at night at both locations (Figures 3c and 3f). Both Namche and Pheriche are located on the valley floor, which is likely to account for the directional consistency in the observed and model winds (Figures 3a, 3b, 3d, and 3e). The downslope nighttime winds that appear in a classic valley circulation (Whiteman, 2000; Zardi & Whiteman, 2013) are not seen in either the model or observations in the summer (Figures 2b and 3b and 3e). This agrees with other studies in the region showing that nighttime downslope winds are not found during the monsoon season (Ohata et al., 1981; Ueno et al., 2001). Note that the model struggled to represent the observed wind at more exposed locations on the mountain peaks of the Dudh Koshi basin (not shown). As the wind at these locations is not governed by the local valley flow, an investigation into the reasons for this is beyond the scope of this study.

At Namche and Pheriche, the main drivers of near-surface wind acceleration (taken from the lowest model level, approximately 25 m above ground) are from the pressure gradient, advection, turbulent vertical mixing, and numerical diffusion (Figures 4c, 4d, 4g, and 4h). There is a clear diurnal cycle in these acceleration components. The drivers generally offset each other; often this occurs between the pressure gradient and one or more of the other forces. Despite Namche and Pheriche both having a relatively strong southerly wind component during the day (Figures 4a and 4b, respectively), considerable differences exist in their respective acceleration components. At Namche, the southerly wind acceleration (deceleration) in the morning (afternoon) is caused by a positive advection component offset by a negative pressure gradient, whereas at Pheriche it is caused by positive advection and pressure gradient, dampened by turbulent vertical mixing and

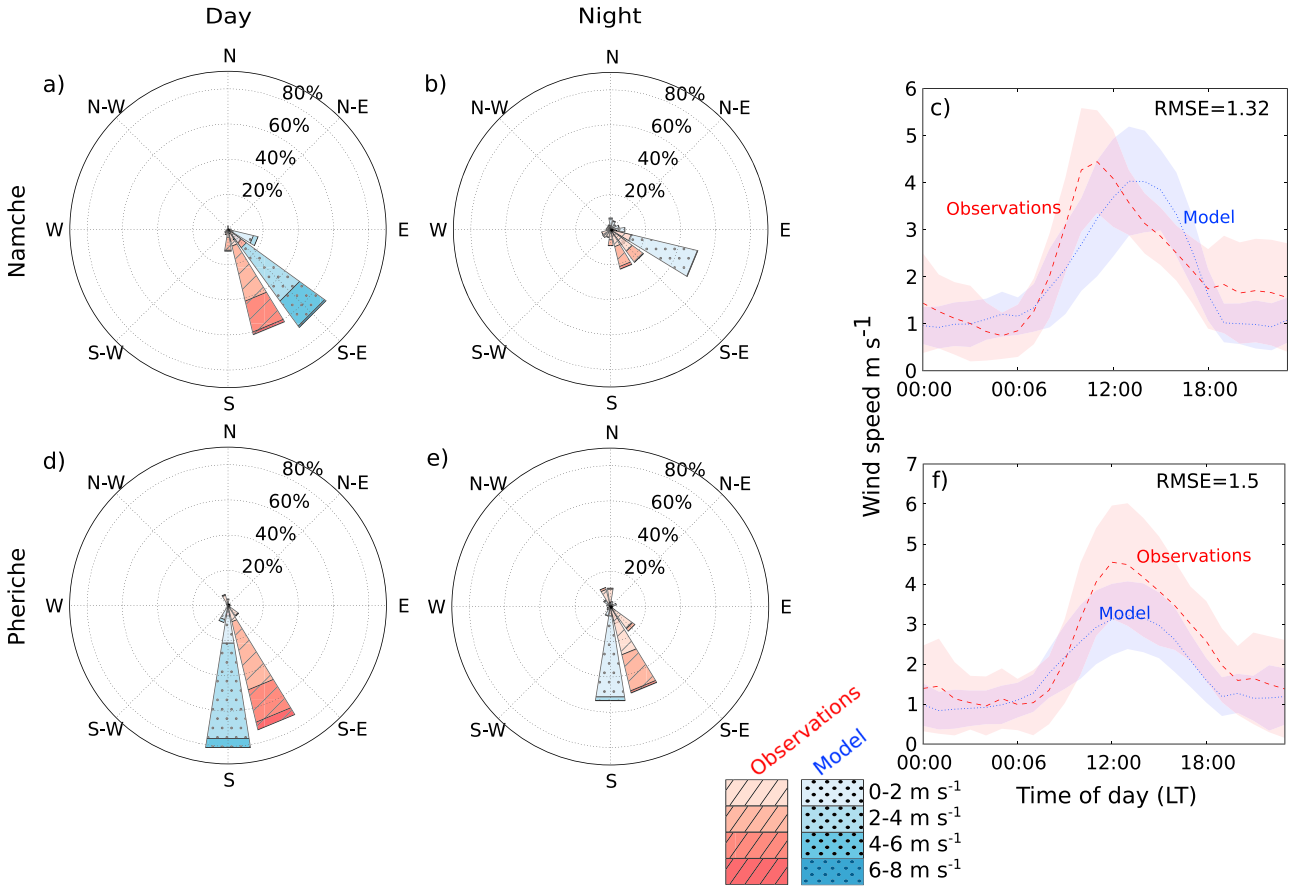

Figure 3. Wind roses comparing the monthly averaged daytime (06:00–18:00 LT) (a) and nighttime (19:00–05:00 LT) (b) observed (red, hatching) and 10 m model (blue, dotted) wind speed and direction at Namche for July 2013. Comparison of the monthly averaged diurnal cycle of observed (red, dashed) and 10 m model (blue, dotted) wind speed (m/s) (c) at Namche for July 2013, with the shading indicating one standard deviation from the mean, and the RMSE shown. Panels (d)–(f) are as (a)–(c), but for Pheriche. The observed wind has been adjusted to 10 m. RMSE = root-mean-square error.

numerical diffusion (Figures 4c and 4d, respectively). The pattern in the acceleration components at Namche is due to the southerly wind being blocked by a hill just to the north of the AWS, leading to a strong negative horizontal velocity gradient and therefore a positive advection term and negative pressure gradient term during the day. In the zonal flow there is also high consistency in the diurnal cycle of the wind and the acceleration components over the month, and differences in these acceleration components between the two sites (Figure 4g and 4h).

The dominance of the pressure gradient, advection, turbulent vertical mixing, and numerical diffusion is seen over the entire Dudh Koshi river basin (Figure 5). As would be expected from previous studies of valley circulations (Zardi & Whiteman, 2013), the largest component of the acceleration causing the up-valley daytime winds seen in Figure 2 comes from the pressure gradient term. This is followed by numerical diffusion (despite it having only a small effect on the wind at Namche and Pheriche (Figure 4)), and then advection and turbulent vertical mixing. At night, the pressure gradient, numerical diffusion, and advection terms are the largest. The acceleration components are extremely variable over the river basin (not shown), and also affected by the presence of snow and ice (see section 3.3).

Figure 6 examines the vertical distribution of the zonal and meridional wind components and the associated momentum budget terms at Namche, Pheriche, and the average over the entire valley during the day. At night away from the surface, the pattern is similar but smaller in magnitude, and so not shown. At Namche and Pheriche, the advection, pressure gradient, and numerical diffusion components are the dominant drivers of the horizontal wind acceleration (excluding near the surface) up to 5,000 m into the atmosphere in both the meridional and zonal directions (Figures 6d, 6e, 6j, and 6k). Despite being less than 10 km apart, the vertical profiles at Namche and Pheriche show different patterns of acceleration components in the troposphere.

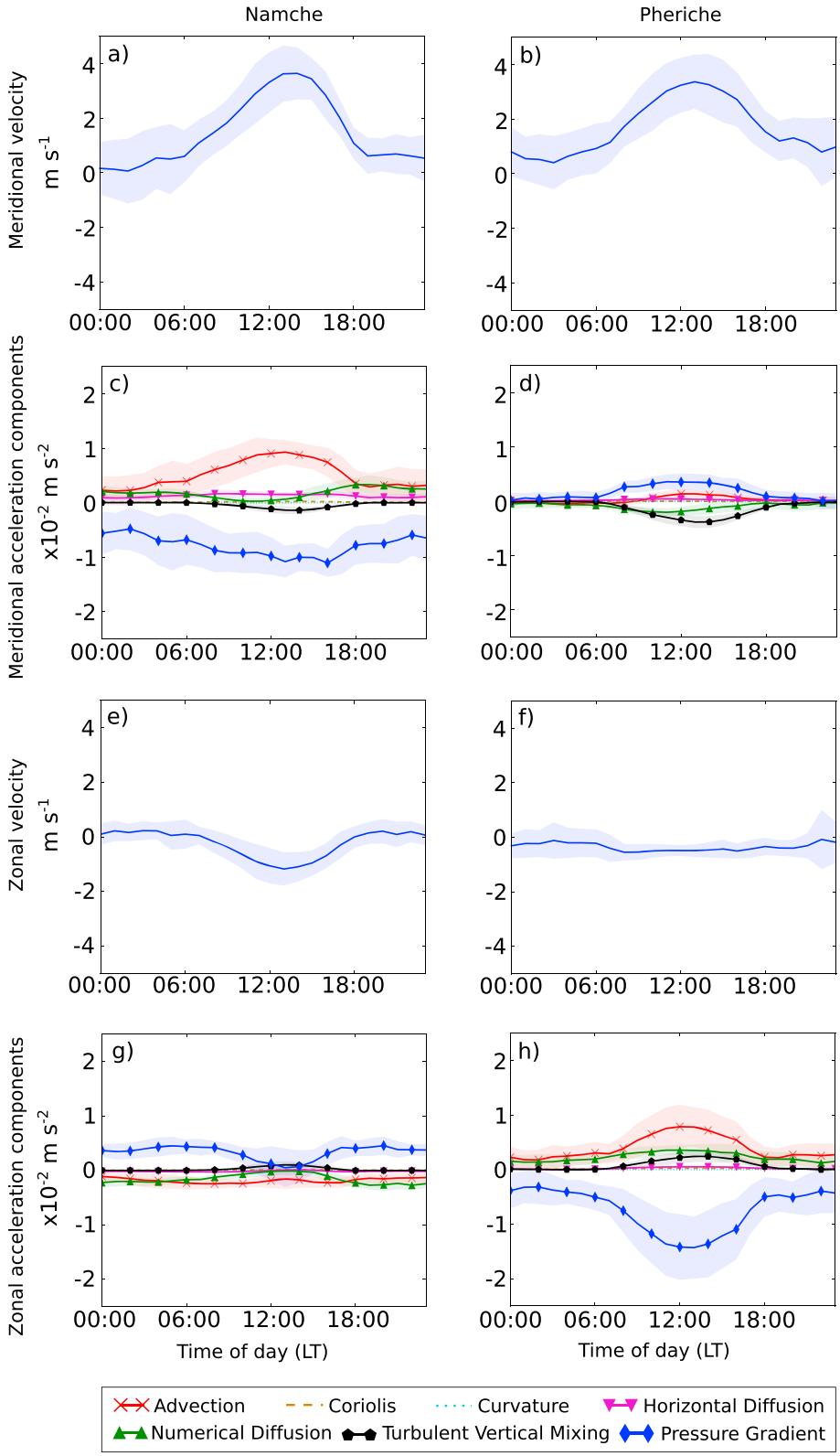

Figure 4. The monthly averaged diurnal cycle of the meridional wind component (m/s) at Namche (a) and Pheriche (b), and the associated acceleration terms (m/s^2) at Namche (c) and Pheriche (d), taken from the lowest model vertical level for July 2013. Panels (e)–(h) are as (a)–(d), but for the zonal wind component and acceleration terms.

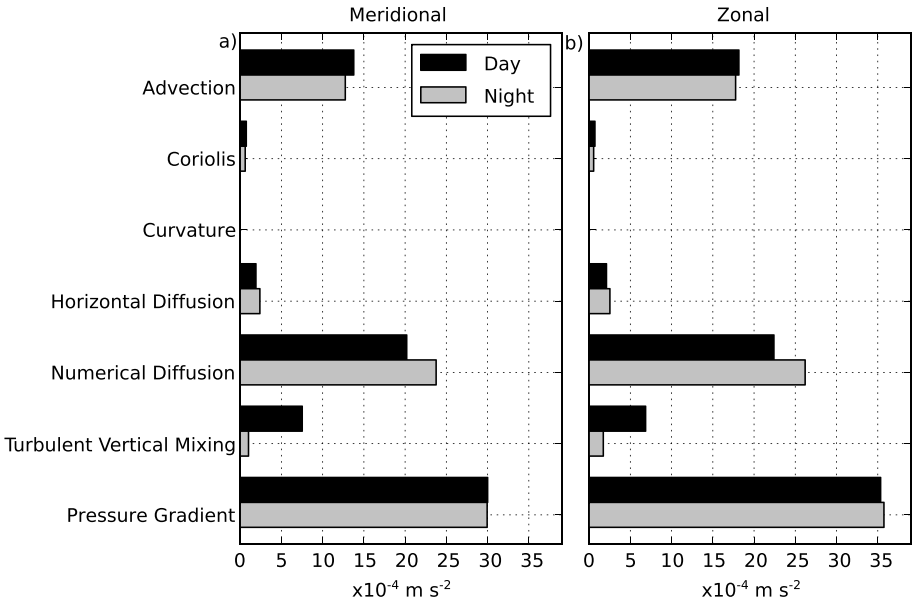

Figure 5. The monthly and valley averaged absolute contributions of each momentum budget component to the wind acceleration (m/s^2) at the lowest model level for July 2013. The components are shown in the meridional (a) and zonal (b) directions averaged over the day (06:00–18:00 LT; black bars) and night (19:00–05:00 LT; gray bars). The valley average has been taken over the area shown in Figure 2, beginning from 27.43°N to avoid boundary issues.

Further analysis (not shown) suggests that this is likely due to small-scale orographic gravity waves, which are trapped (e.g., Alexander et al., 2017) due to the background wind speed increasing with height, as is evident in Figures 6g–6i. When averaged over the entire valley, the momentum budget components approach a quasi-geostrophic balance between the Coriolis term and the pressure gradient term, although there is still a contribution from the advection term (Figures 6f and 6l).

At Namche there is a low-level jet structure in the meridional wind component, with a maximum velocity at about 300 m above the ground (Figure 6a), which is predominantly accelerated by a positive advection component offset by a negative pressure gradient (Figure 6d). This pattern of advection offset by pressure gradient continues to almost 2,000 m above the ground at Namche, above which there is a crossover point where the pressure gradient and advection terms switch signs.

At Pheriche, the maximum meridional velocity is near the surface (Figure 6b), but here the positive pressure gradient term is offset by negative numerical diffusion and turbulent vertical mixing terms, which switch sign at about 200 m (Figure 6e). There is another switch at about 1,500 m. As Pheriche is approximately 700 m higher than Namche, the 1,500–2,000 m crossover points represent similar altitudes at both sites, and, as such, indicate a change in forcing from inside the valley to the free atmosphere. The pressure gradient (and advection) term is much larger below this crossover point than above it, particularly in the meridional direction at Namche and the zonal direction at Pheriche. This suggests that the near-surface pressure gradient examined in Figure 4 is caused by local pressure gradients rather than synoptic pressure gradients in the summer. The dominance of the local pressure gradient over the synoptic pressure gradient was confirmed by splitting the pressure gradient into its local and synoptic components, following the method used by Moisseeva and Steyn (2014) (not shown). The crossover point is less clear in the valley averaged momentum budget component, due to the height above the ground being averaged over the full valley, however above about 2,500 m the momentum budget components represent the free atmosphere (Figures 6f and 6l).

3.2. Winter

Along the valley floor, the pattern in the near-surface winds in the model output in the winter run is similar to that in the summer run; up-valley winds during the day and the wind subsiding at night (Figures 2c and 2d). However, at high elevations the winter pattern is different to that of the summer, with strong westerly winds throughout the day and night (Figures 2c and 2d). Additionally, in the summer run the up-valley winds continue up to (or just over) the permanent snow and ice outline during the day in the north of the valley (Figure 2a). However, in the winter run, the up-valley winds subside before the glaciers, and in this region

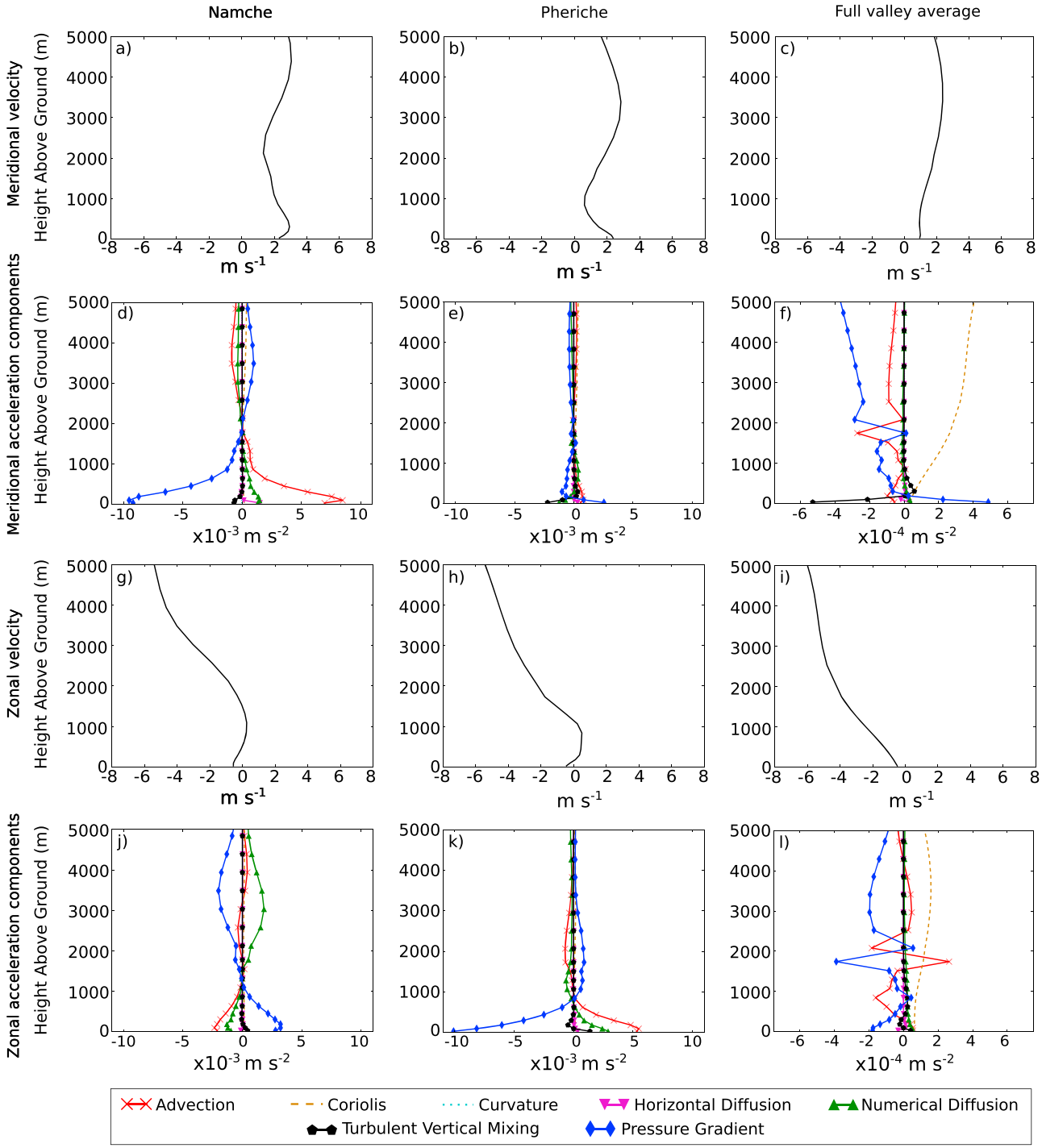

Figure 6. The monthly averaged daytime (06:00–18:00 LT) vertical distribution of the model meridional wind component (m/s) at Namche (a), Pheriche (b), and averaged over the entire valley (c) for July 2013. Panels (d)–(f) show the associated acceleration terms (m/s^2) at Namche, Pheriche, and the valley average, respectively. Panels (g)–(l) are as (a)–(f), but for the zonal wind component and associated acceleration terms. Note the change in scale in panels (f) and (l). The valley average has been taken over the area shown in Figure 2, beginning from 27.43°N to avoid boundary issues.

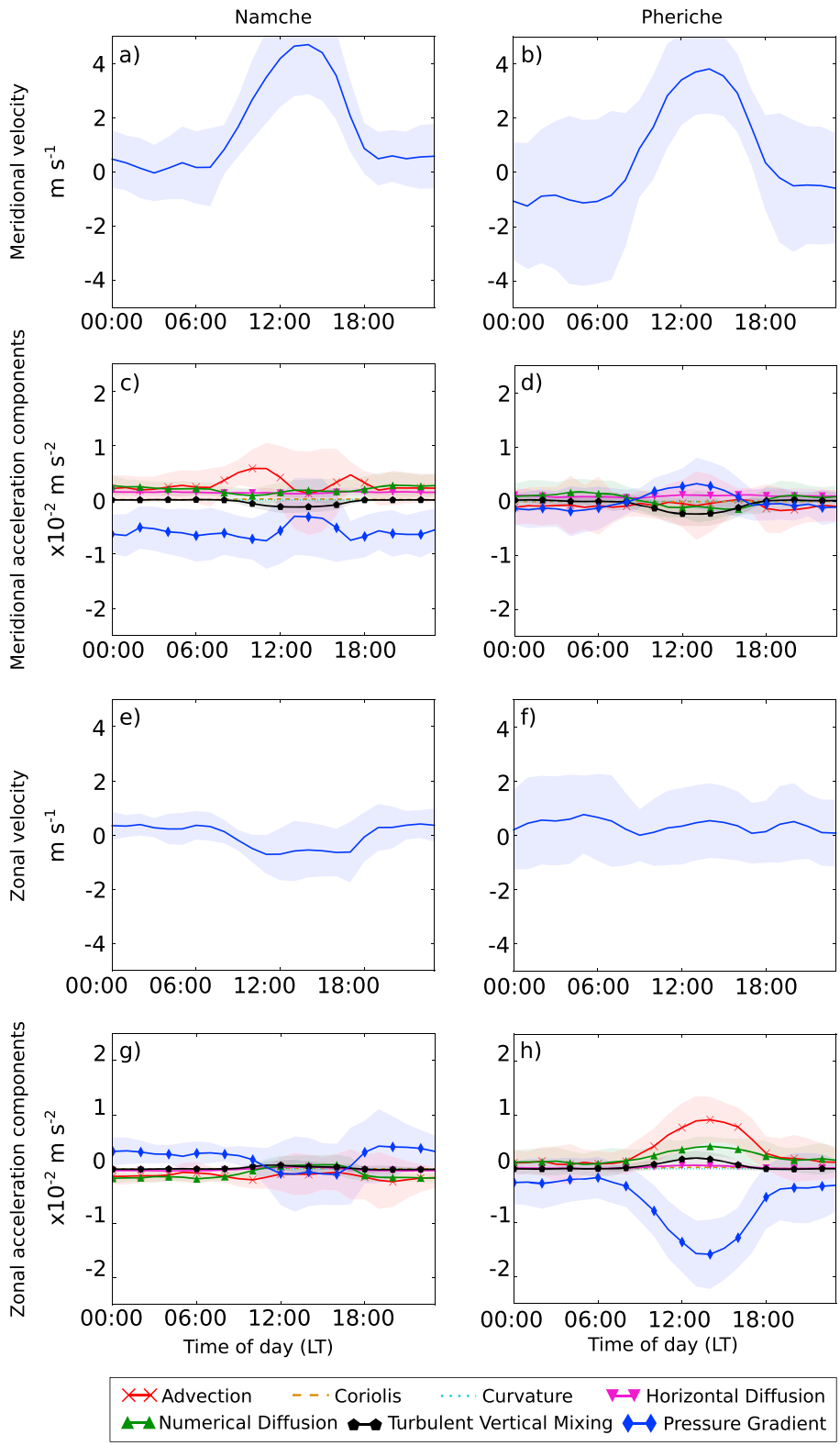

Figure 7. As Figure 4, but for January 2014.

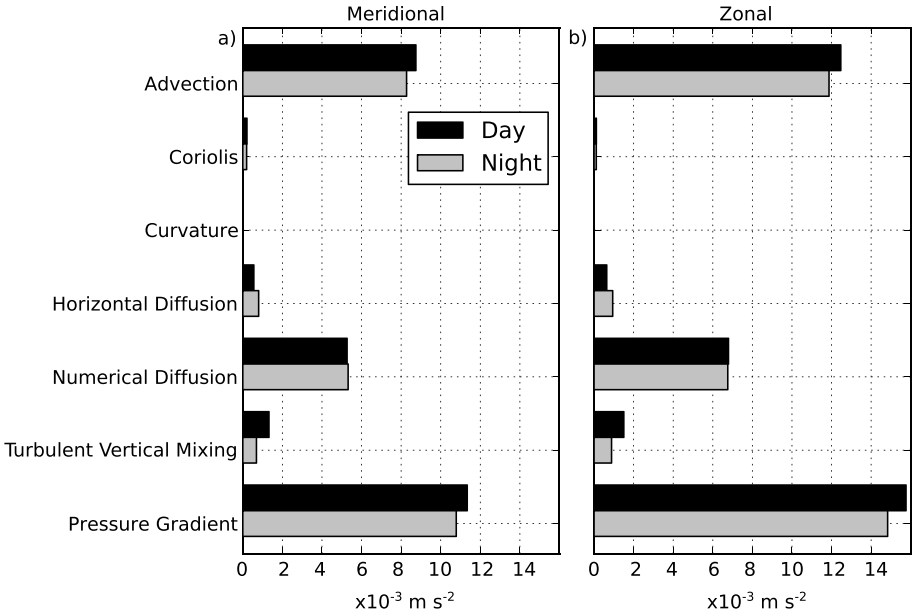

Figure 8. As Figure 5, but for January 2014. Note the change of scale. Daytime is taken as 07:00–17:00 LT in the winter run.

alone we see the downslope nighttime winds of a classic diurnal circulation (Figure 2d). As in the summer run, the model represents the wind speed and direction relatively well in winter at Namche and Pheriche, with a root-mean-square error for wind speed of 1.15 and 1.82 m/s, respectively. The wind directions are broadly similar to those in the summer (slightly more southerly than in the summer, with slightly more variation in both the model and observations) and as such are not shown.

The similarity between the winter and summer runs in the winds along the valley floor is also seen in the wind speed and acceleration components at Namche and Pheriche. In both directions and at both locations, there is still a clear diurnal cycle in the winds with stronger winds during the day, and much weaker winds at night (Figures 7a, 7b, 7e, and 7f), of broadly similar magnitudes to the wind speeds in the summer run. In addition, the patterns in the acceleration components are similar at Namche and Pheriche in the winter to those seen in the summer (Figure 7c, 7d, 7g, and 7h). However, the diurnal cycle in both the wind speeds and the acceleration components is less consistent in the winter run (Figure 7) compared to the summer run (Figure 4).

Over the entire valley, every component of near-surface acceleration is larger in the winter run than in the summer run, in both the meridional and zonal directions (Figure 8). The pressure gradient is still the largest term. The advection term surpasses the numerical diffusion term to become the second biggest term, but the pressure gradient, advection, numerical diffusion, and turbulent vertical mixing terms remain the largest terms during the day.

The most noticeable difference in the vertical distribution of the acceleration components in the winter run compared to the summer run is the increase in wind speed at high altitudes, especially in the zonal direction, where wind speeds reach above 40 m/s (Figures 9g–9l, cf. Figures 6g–6l), demonstrating the influence of the winter westerlies. The drivers in the wind acceleration at Namche and Pheriche are also larger at high altitudes in the winter run than the summer run, but the pressure gradient, advection, numerical diffusion, and Coriolis terms remain the largest terms (Figures 9d, 9e, 9j, and 9k, cf. Figures 6d, 6e, 6j, and 6k). There is a larger contribution (and a switch in sign) from the Coriolis acceleration in the meridional direction in the winter compared to the summer due to the switch in direction and increase in zonal wind at high altitudes. Due to the increase in the magnitude of the drivers at high altitudes, and the variability of the pressure gradient throughout the atmospheric column, it is not possible to determine whether the near-surface pressure gradient is predominantly locally or synoptically forced in the winter. However, the crossover point in the acceleration components indicates a difference in the mechanisms driving the winds in the valley compared to the free atmosphere (Figures 9d–9f, 9j–9l).

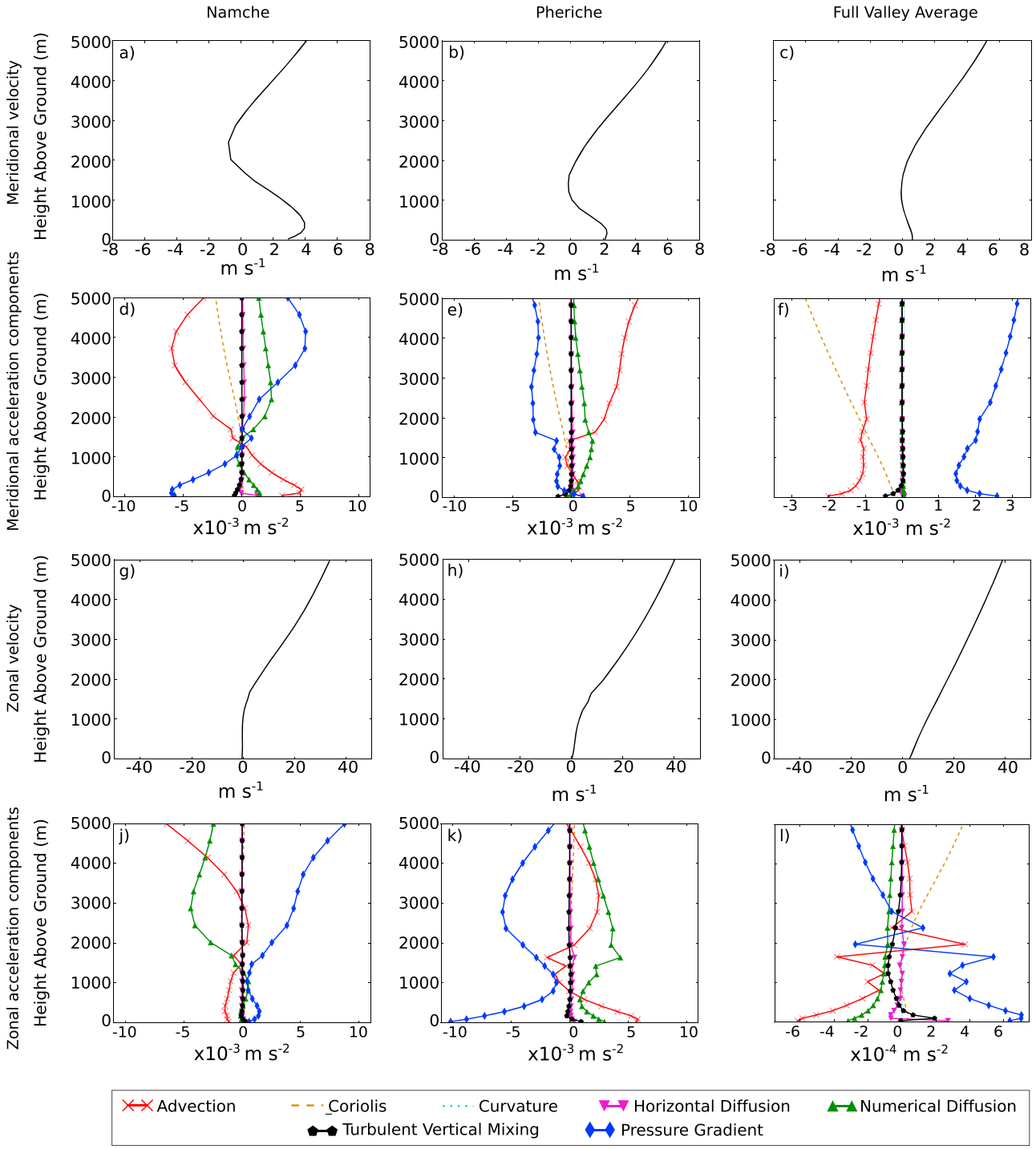

Figure 9. As Figure 6, but for January 2014. Note the change of scale in the zonal velocity and panels (f) and (l). Daytime is taken as 07:00–17:00 LT in the winter run.

3.3. Removal of Glacierized Region

Figure 2, and maps of each of the acceleration terms (not shown), indicate that the wind and the drivers of the wind acceleration are extremely variable over the valley, and also influenced by the presence of permanent snow and ice. In this section we investigate the role of glacier coverage by examining the results of the perturbation experiments. In the summer run, the daytime up-valley winds are weakened over the glaciers (Figure 2a). However, in the summer perturbation experiment, when the glaciers are removed from the valley,

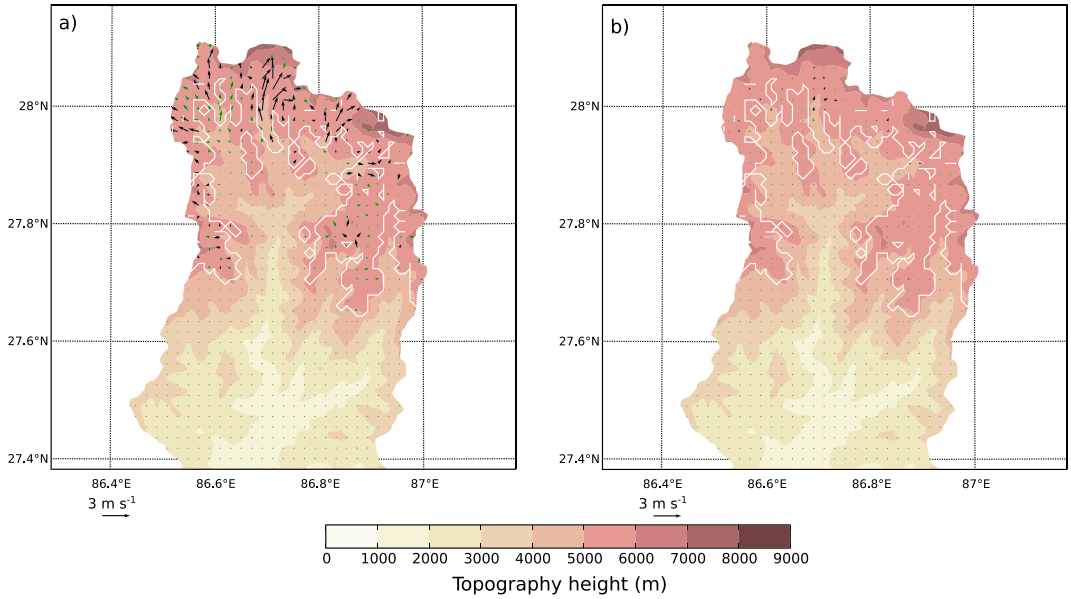

Figure 10. The monthly averaged daytime (06:00–18:00 LT) (a) and nighttime (19:00–05:00 LT) (b) difference in the 10 m winds for July 2013 between the summer perturbation experiment and the summer run (perturbation experiment-summer run). Significant vector differences are shown in black, nonsignificant differences are shown in green. Wind vectors are displayed at every second model grid point (every 2 km) for clarity. Also shown are the model topographic height (m; shading) and the previous extent of the permanent snow and ice in the model (solid white line). Note the change in scale compared to Figure 2.

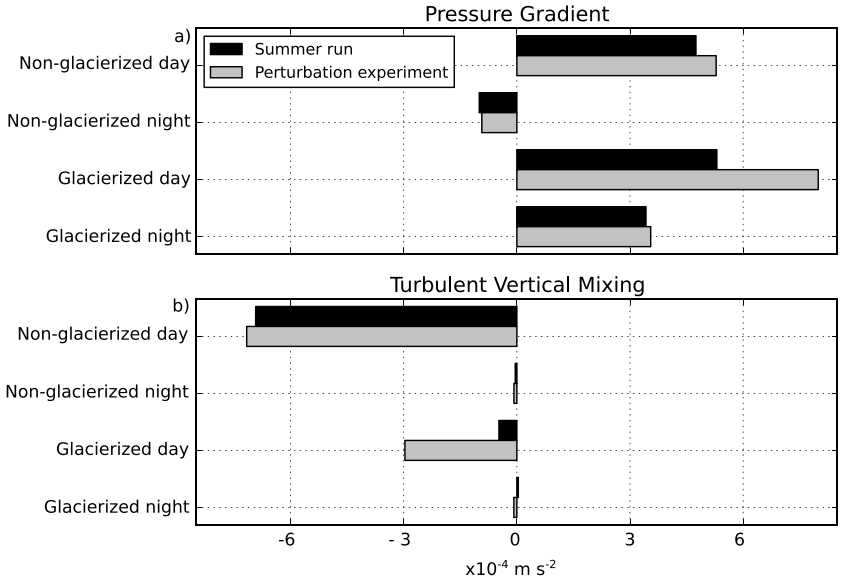

Figure 11. The meridional acceleration component of the pressure gradient (a) and the turbulent vertical mixing (b) terms, averaged over the glacierized and nonglacierized regions of the valley for the day (06:00–18:00 LT) and night (19:00–05:00 LT) for July 2013. The valley average has been taken over the area shown in Figure 2, for the glacierized and nonglacierized regions (bounded by the white line), beginning from 27.43°N to avoid boundary issues. The summer run is shown in black and the summer perturbation experiment is shown in gray. A positive value indicates a south to north acceleration (mostly up-valley) over the region.

the daytime up-valley winds continue to the top of the river basin (Figure 10a), demonstrating that the winds are currently being damped by the glaciers, rather than, for example, by the increasing topographical gradient. There is no consistent difference seen in the winds between the winter run and the winter perturbation experiment (not shown).

For both the summer run and the summer perturbation experiment, the pressure gradient generally accelerates the wind up-valley during the day (Figure 11a). Over the currently nonglacierized parts of the valley, there is a strong diurnal cycle in the pressure gradient, with a large southerly (up-valley) acceleration from the pressure gradient during the day and a small northerly (down-valley) acceleration at night. The diurnal cycle is considerably smaller over the currently glacierized regions than in the currently nonglacierized regions in the summer run, with a small decrease in the southerly acceleration at night (Figure 11a). In the summer perturbation experiment, there is a substantial increase in the up-valley acceleration from the pressure gradient during the day over the currently glacierized areas, in response to the removal of the glaciers. (Figure 11a).

The turbulent vertical mixing term dampens the winds during the day over currently nonglacierized regions in the summer run and the summer perturbation experiment (Figure 11b). Over the currently glacierized areas during the day in the summer run, and over the whole basin at night in both the summer run and summer perturbation experiment, there is very little contribution from turbulent vertical mixing (Figure 11b). In the summer perturbation experiment, there is an increased northerly acceleration (dampening) of the up-valley meridional wind over the areas where the glaciers have been removed. In the summer perturbation experiment, the increase in the up-valley acceleration from the pressure gradient is larger than the dampening from the turbulent vertical mixing, leading to the increase in winds seen in Figure 10. The other drivers do not show a substantial change in the summer perturbation experiment compared to the summer run when averaged over the currently glacierized area.

4. Discussion and Conclusions

In this paper we run the WRF model at 1 km resolution over the Dudh Koshi river basin in the Nepalese Himalaya for July 2013 and January 2014. We find that the model accurately represents the near-surface wind speed and direction at two AWSs located in the valley. In the summer there is a clear diurnal cycle in the near-surface winds over the nonglacierized areas of the valley, with strong up-valley winds during the day and weak winds at night, confirming previous findings (Inoue, 1976; Ohata et al., 1981; Shea, Wagnon, et al., 2015; Ueno et al., 2001; Yang et al., 2017). In the winter the winds at lower elevations in the valley show a similar pattern to those in the summer, however at high elevations there is an influence from the synoptic scale winter westerly winds. Previous work has suggested that in winter, a classic local wind regime is seen in this valley, with downslope winds in the nighttime (Yang et al., 2017). In this study, we find that this is only true of the wind just below the glacier margins, and does not hold further down the valley where weak up-valley nighttime winds predominate. Bollasina et al. (2002) found weak downslope winds during winter in the nighttime at the Pyramid station, which is located just on the glacier margin. Our findings agree with this study; the model shows nighttime downslope winds at this location in the winter. Our study partially supports the findings of Ueno et al. (2008), who found very weak nighttime winds in winter at lower elevations of the valley, but our results are not consistent with their finding of nighttime downslope winds at Pheriche in the winter of January 2003.

Using a momentum budget analysis of the WRF output, we show that the dominant drivers of the near-surface horizontal wind acceleration in the summer are the pressure gradient, advection, turbulent vertical mixing, and the nonphysical numerical diffusion term. These drivers also show a clear diurnal cycle. Although the interplay between the terms is complex, typically the pressure gradient term dominates. Examining the vertical distribution of the pressure gradient suggests that in the summer the near-surface pressure gradient is caused mostly by local rather than synoptic pressure gradients. The drivers of near-surface wind acceleration are extremely variable over the valley and also affected by the presence of glaciers. When the glaciers are removed from the model in the summer, there is an increase in the pressure gradient which causes the up-valley winds to continue to the top of the valley during the day, although the winds are partially damped by an increase in northerly acceleration from turbulent vertical mixing.

Compared to the summer, the magnitude of all the acceleration components increases in the winter, particularly at high altitudes, and there is a more variable diurnal cycle in the wind and the dynamical drivers near the surface. The influence of the winter westerlies is seen in the model at high altitudes at Namche and Pheriche.

In both the summer and the winter runs, the vertical components of the momentum budget switch sign (or drop to zero) approximately 1,500–2,000 m above the ground, suggesting that there is a distinction between the drivers of the wind acceleration inside the valley and in the free atmosphere. Orographic gravity waves affect the vertical distribution of acceleration terms at Namche and Pheriche. However, when the momentum budget components are averaged over the valley, they approach a quasi-geostrophic balance at high altitudes.

The high spatial variability of the wind acceleration components and the dominance of the pressure gradient both result from the impact of the tremendously complex terrain that characterizes the Dudh Koshi river basin as well as the wider HKKH region, which requires modeling with a resolution of around 1 km in order to realize accurate output (Collier & Immerzeel, 2015; Karki et al., 2017; Orr et al., 2017; Zängl et al., 2001). The importance of the local pressure gradient and turbulent vertical mixing additionally informs us that the representation of the land surface (and planetary boundary layer) to compute heat and moisture fluxes is crucial to produce accurate results in the near-surface wind field. This requires accurate representation of the input land cover field, and particularly the glacier coverage. As the glaciers melt in the region, we are likely to see summer daytime up-valley winds continuing further up the valley due to the increase in the pressure gradient, and this will affect other meteorological variables, such as cloud cover, incoming radiation, and precipitation. These results have implications for our understanding not only of local winds, but also the wider glacio-hydro-meteorological system, including glacier mass balance and river runoff, in valleys over the HKKH region. Studies such as this should therefore be extended to focus on other river basins throughout the HKKH region in order to better understand the drivers of these winds.

Acknowledgments
First, we would like to thank the three anonymous reviewers for their valuable contributions to the manuscript, which have hugely improved it. Many thanks to Pierre Chevallier for collating the observational data and also to Elisa Vuillermoz. The code for the bootstrap statistical significance test was provided by Christine McKenna. We would also like to thank John King, Alison Ming, Patrick Wagnon, and Francesca Pellicciotti for their advice with this study. The code used to alter the WRF model can be found at https://github.com/Empott/WRF-momentum-and-temperature-budget-variables, and was based on the code and instructions provided by Nadejda Moisseeva at https://open.library.ubc.ca/media/download/pdf/33426/1.0107646/1. The model data can be accessed at https://doi.org/10.5285/4b825de1a86e42dbb7abe1f65dcd9abd and https://doi.org/10.5285/49ff98246c1f42d7bc0046ae4d0b7ea8. The funding for this project was provided by the National Environmental Research Council, grant NE/L002507/1.

References

Alexander, S., Orr, A., Webster, S., & Murphy, D. (2017). Observations and fine-scale model simulations of gravity waves over Davis, East Antarctica (69°S, 78°E). *Journal of Geophysical Research: Atmospheres*, *122*, 7355–7370. https://doi.org/10.1002/2017JD026615

Bollasina, M., Bertolani, L., & Tartari, G. (2002). Meteorological observations at high altitude in the Khumbu Valley, Nepal Himalayas, 1994–1999. *Bulletin of Glaciological Research*, *19*, 1–12.

Chandler, R., & Scott, M. (2011). *Statistical methods for trend detection and analysis in the environmental sciences*. Chichester: John Wiley.

Collier, E., & Immerzeel, W. W. (2015). High-resolution modeling of atmospheric dynamics in the Nepalese Himalaya. *Journal of Geophysical Research: Atmospheres*, *120*, 9882–9896. https://doi.org/10.1002/2015JD023266

Collins, W. D., Rasch, P. J., Boville, B. A., Hack, J. J., McCaa, J. R., Williamson, D. L., et al. (2004). Description of the NCAR community atmosphere model (CAM 3.0) (Tech. Rep.). Boulder, CO: National Center For Atmospheric Research.

Consortium, R. (2015). Randolph Glacier Inventory — A dataset of global glacier outlines: Version 5.0 (Tech. Rep.) Colorado, USA: Global Land Ice Measurements from Space.

Dee, D. P., Uppala, S., Simmons, A., Berrisford, P., Poli, P., Kobayashi, S., et al. (2011). The ERA-interim reanalysis: Configuration and performance of the data assimilation system. *Quarterly Journal of the Royal Meteorological Society*, *137*(656), 553–597.

Egger, J., Bajrachaya, S., Heinrich, R., Kolb, P., Lämmlein, S., Mech, M., et al. (2002). Diurnal winds in the Himalayan Kali Gandaki valley. Part III: Remotely piloted aircraft soundings. *Monthly Weather Review*, *130*(8), 2042–2058.

Immerzeel, W., Petersen, L., Ragettli, S., & Pellicciotti, F. (2014). The importance of observed gradients of air temperature and precipitation for modeling runoff from a glacierized watershed in the Nepalese Himalayas. *Water Resources Research*, *50*, 2212–2226. https://doi.org/10.1002/2013WR014506

Inoue, J. (1976). Climate of Khumbu Himal. *Journal of the Japanese Society of Snow and Ice*, *38*(Special), 66–73.

Jarvis, A., Reuter, H. I., Nelson, A., & Guevara, E. (2008). Hole-filled SRTM for the globe version 4. available from the CGIAR-CSI SRTM 90m Database (http://srtm. csi. cgiar. org), 15.

Jiménez, P. A., Dudhia, J., González-Rouco, J. F., Navarro, J., Montávez, J. P., & García-bustamante, E. (2012). A revised scheme for the WRF surface layer formulation. *Monthly Weather Review*, *140*(3), 898–918.

Karki, R., ul Hasson, S., Gerlitz, L., Schickhoff, U., Scholten, T., & Böhner, J. (2017). Quantifying the added value of convection-permitting climate simulations in complex terrain: A systematic evaluation of WRF over the Himalayas. *Earth System Dynamics*, *8*(3), 507–528. https://doi.org/10.5194/esd-8-507-2017

Lehner, M. (2012). Observations and large-eddy simulations of the thermally driven cross-basin circulation in a small closed basin (PhD thesis), The University of Utah.

Lehner, M., & Whiteman, C. D. (2014). Physical mechanisms of the thermally driven cross-basin circulation. *Quarterly Journal of the Royal Meteorological Society*, *140*(680), 895–907.

Ma, L.-M., & Tan, Z.-M. (2009). Improving the behavior of the cumulus parameterization for tropical cyclone prediction: Convection trigger. *Atmospheric Research*, *92*(2), 190–211.

Magnani, A., Ajmone-Marsan, F., D'Amico, M., Balestrini, R., Viviano, G., Salerno, F., & Freppaz, M. (2018). Soil properties and trace elements distribution along an altitudinal gradient on the southern slope of Mt. Everest, Nepal. *CATENA*, *162*, 61–71.

Moisseeva, N. (2014). Dynamical analysis of sea breeze hodograph rotation in Sardinia (Master's thesis), University of British Columbia.

Moisseeva, N., & Steyn, D. (2014). Dynamical analysis of sea-breeze hodograph rotation in Sardinia. *Atmospheric Chemistry and Physics*, *14*(24), 13,471–13,481.

Morrison, H., Thompson, G., & Tatarskii, V. (2009). Impact of cloud microphysics on the development of trailing stratiform precipitation in a simulated squall line: Comparison of one-and two-moment schemes. *Monthly Weather Review*, *137*(3), 991–1007.

Nakanishi, M., & Niino, H. (2004). An improved Mellor–Yamada level-3 model with condensation physics: Its design and verification. *Boundary-Layer Meteorology*, *112*(1), 1–31.

Niu, G.-Y., Yang, Z.-L., Mitchell, K. E., Chen, F., Ek, M. B., Barlage, M., et al. (2011). The community Noah land surface model with multiparameterization options (Noah-MP): 1. Model description and evaluation with local-scale measurements. *Journal of Geophysical Research*, *116*, D12109. https://doi.org/10.1029/2010JD015139

Ohata, T., Higuchi, K., & Ikegami, K. (1981). Mountain-valley wind system in the Khumbu Himal, East Nepal. *Journal of the Meteorological Society of Japan. Ser. II*, *59*(5), 753–762.

Oke, T. R. (2002). *Boundary layer climates*. Abingdon, Oxon: Taylor & Francis.

Orr, A., Listowski, C., Couttet, M., Collier, E., Immerzeel, W., Deb, P., & Bannister, D. (2017). Sensitivity of simulated summer monsoonal precipitation in Langtang Valley, Himalaya, to cloud microphysics schemes in WRF. *Journal of Geophysical Research: Atmospheres*, *122*, 6298–6318. https://doi.org/10.1002/2016JD025801

Pritchard, H. D. (2017). Asia's glaciers are a regionally important buffer against drought. *Nature*, *545*(7653), 169–174.

Renfrew, I. A. (2004). The dynamics of idealized katabatic flow over a moderate slope and ice shelf. *Quarterly Journal of the Royal Meteorological Society*, *130*(598), 1023–1045.

Salerno, F., Thakuri, S., Tartari, G., Nuimura, T., Sunako, S., Sakai, A., & Fujita, K. (2017). Debris-covered glacier anomaly? Morphological factors controlling changes in the mass balance, surface area, terminus position, and snow line altitude of Himalayan glaciers. *Earth and Planetary Science Letters*, *471*, 19–31.

Shea, J., Immerzeel, W., Wagnon, P., Vincent, C., & Bajracharya, S. (2015). Modelling glacier change in the Everest region, Nepal Himalaya. *The Cryosphere*, *9*(3), 1105–1128.

Shea, J. M., Wagnon, P., Immerzeel, W. W., Biron, R., Brun, F., & Pellicciotti, F. (2015). A comparative high-altitude meteorological analysis from three catchments in the nepalese himalaya. *International journal of water resources development*, *31*(2), 174–200.

Skamarock, W., Klemp, J., Dudhia, J., Gill, D., Barker, D., Wang, W., & Powers, J. (2008). A Description of Theadvanced Research Wrf Version 3 (Tech. Rep). NCAR.

Sun, F., Ma, Y., Hu, Z., Li, M., Tartari, G., Salerno, F., et al. (2018). Mechanism of daytime strong winds on the northern slopes of himalayas, near mount everest: Observation and simulation. *Journal of Applied Meteorology and Climatology*, *57*(2), 255–272.

Tartari, G., Verza, G., & Bertolami, L. (1998). Meteorological data at the pyramid observatory laboratory (khumbu valley, sagarmatha national park, nepal). *Mem. Ist. Ital. Idrobiol*, *57*, 23–40.

Ueno, K., Kayastha, R., Chitrakar, M., Bajracharya, O., Pokhrel, A., Fujinami, H., et al. (2001). Meteorological observations during 1994-2000 at the automatic weather station (gen-aws) in khumbu region, Nepal himalayas. *Bulletin of Glacier Research*, *18*, 23–30.

Ueno, K., Toyotsu, K., Bertolani, L., & Tartari, G. (2008). Stepwise onset of monsoon weather observed in the Nepal himalaya. *Monthly Weather Review*, *136*(7), 2507–2522.

van Angelen, J. H., van den Broeke, M. R., & van de Berg, W. J. (2011). Momentum budget of the atmospheric boundary layer over the Greenland ice sheet and its surrounding seas. *Journal of Geophysical Research*, *116*, D10101. https://doi.org/10.1029/2010JD015485

van den Broeke, M., van Lipzig, N., & van Meijgaard, E. (2002). Momentum budget of the east antarctic atmospheric boundary layer: Results of a regional climate model. *Journal of the Atmospheric Sciences*, *59*(21), 3117–3129.

von Storch, H., & Zwiers, F. W. (1999). *Statistical Analysis in Climate Research*. Cambridge: Cambridge University Press.

Wagnon, P., Vincent, C., Arnaud, Y., Berthier, E., Vuillermoz, E., Gruber, S., et al. (2013). Seasonal and annual mass balances of mera and pokalde glaciers (nepal himalaya) since 2007. *The Cryosphere*, *7*(6), 1769–1786.

Whiteman, C. D. (2000). *Mountain Meteorology: Fundamentals and Applications*. New York: Oxford University Press.

Widmann, M., Blake, R., Sooraj, K., Orr, A., Sanjay, J., Karumuri, A., et al. (2017). Current opportunities and challenges in developing hydro-climatic services in the Himalayas. IUKWC report.

Yang, K., Guyennon, N., Ouyang, L., Tian, L., Tartari, G., & Salerno, F. (2017). Impact of summer monsoon on the elevation-dependence of meteorological variables in the south of central himalaya. *International Journal of Climatology*, *38*, 1748–1759. https://doi.org/10.1002/joc.5293

Zängl, G., Egger, J., & Wirth, V. (2001). Diurnal winds in the himalayan kali gandaki valley. Part II: Modeling. *Monthly Weather Review*, *129*(5), 1062–1080.

Zardi, D., & Whiteman, C. D. (2013). Diurnal mountain wind systems. In F. K. Chow, S. F. J. De Wekker, & B. J. Snyder (Eds.), *Mountain Weather Research and Forecasting* (pp. 35–119). Dordrecht, New York: Springer.